

PAPER NAME

## plagiarism check modified.docx

WORD COUNT CHARACTER COUNT

6767 Words 41620 Characters

PAGE COUNT FILE SIZE

40 Pages 7.0MB

SUBMISSION DATE REPORT DATE

May 30, 2023 4:20 PM GMT+5:30 May 30, 2023 4:20 PM GMT+5:30

#### 9% Overall Similarity

The combined total of all matches, including overlapping sources, for each database.

- 3% Internet database
- Crossref database
- 3% Submitted Works database

- 5% Publications database
- Crossref Posted Content database

## Excluded from Similarity Report

- · Bibliographic material
- · Cited material

- Quoted material
- Small Matches (Less then 10 words)

## 1. Introduction

The need for various sources of energy is growing day by day in modern human civilization. A variety of sources, including coal, petroleum, and others, can be utilized to create various types of energy. As a result, the demand for such sources is growing, yet these resources are being depleted due to overpopulation. To create energy, we need non-traditional or green resources. Various academics and experts are concentrating on the creation of energy or electricity from non-conventional sources. At the same time, piezoelectric materials are being investigated due to their unique features. Solar energy, piezoelectric energy (mechanical pressure - energy), tidal energy, and other types of energy are utilized. Among these is the extraction of energy from various piezoelectric materials. These materials are crucial for the measurement of pressure and harvesting of energy [1]. These materials are sensitive in nature and they are also important for artificial intelligence for obtaining environmental parameters like pressure, light, temperature, and voice. There are various types of piezoelectric ceramics like Pb (Zr, Ti) O<sub>3</sub> (PZT)-centric piezoceramics, NKN-centric ceramics ((Na, K) NbO<sub>3</sub>-BaTiO<sub>3</sub> or (NKN-BT))[2-4], (Na, K) NbO<sub>3</sub>-LiNbO<sub>3</sub>-AgTaO<sub>3</sub>, etc.). In earlier research Pbcontaining ceramics (PZT) are used very commonly due to their excellent multifunctional ceramic attributes compared to other functional ceramics [5-8]. Taking into account the toxic nature of lead oxide in lead-based ceramics is harmful to humans and also ecotoxic. Due to toxicity of Pb, the use of Pb-based ceramics in electrical appliances is banned in the future. As a result, lead-free ceramics with outstanding piezoelectric, ferroelectric, and dielectric characteristics are required. Recent research has discovered certain non-toxic perovskite ceramics with high-quality piezoelectric and ferroelectric capabilities, especially (Na, K) NbO<sub>3</sub> (NKN) and (Bi, Na) TiO<sub>3</sub> (BNT) [9-12]. KNN ceramics with perovskite structures have been proposed as a possible lead-free material replacement to PZT [13-16]. Because of its high dielectric constant, high curie temperature, cost-effectiveness, lead-free and environmental friendliness, good piezoelectric capabilities, and exceptional future potential, KNN-LiSb  $\{(1-x)(K_{0.48}Na_{0.52}) \text{ NbO}_3-x\text{LiSbO}_3)\}$  ceramic was chosen as a filler material in polymers [16-20].

On the contrary, the most effective polymer selection and optimization of fabrication techniques are required to maximize performance in composite generators [21-23]. This approach results in increased elasticity and a monitored processing window, resulting in reliable energy harvesters based on a responsive polymer matrix[24-26]. Many polymers have been employed, including PVDF, its copolymers (P[VDF-TrFE], P[VDF-HFP], P[VDF-TFE], PDMS, and many more. The polyvinylidene fluoride (PVDF) polymer was chosen as the matrix because its crystalline structure includes five different phases, namely,  $\alpha$ ,  $\beta$ ,  $\gamma$ ,  $\delta$ , and  $\varepsilon$  and [27-30]. PVDF's mechanical strength and flexibility are well known. It is lightweight and inexpensive. In comparison to other polymeric polymers such as nylon-11, polypropylene, polydimethylsiloxane, and others, [31-33]. PVDF has a higher piezoelectric coefficient. Mechanical stretching, the inclusion of different filler materials into PVDF material, and the electrospinning operation were used to achieve the  $\beta$ -phase change from  $\alpha$ -phase to  $\beta$ -phase. [34-35].

In this work, lead-free KNN-LiSb ceramic is used as a filler, and a PVDF matrix is used to analyze energy harvesting qualities. A number of characterization methods, including  $^3$ -ray diffraction (XRD), Scanning Electron Microscopy (SEM), and Fourier Transform Infrared Spectroscopy (FTIR), were used to evaluate the composite flexible films used in device manufacture. The piezoelectric properties of the gadget were tested using an electrodynamic shaker. Furthermore, the piezoelectric performance of the device was investigated in relation to KNN-LiSb ceramic concentration. The open-circuitry voltage and short-circuiting current of the device were found out to be 15.47 V and 2.14  $\mu$ A, respectively. The constructed devices in this work show promising characteristics like flexibility, wearability, affordability, and implantability, making them extremely appropriate for energy-harvesting applications.

#### 1.1 Piezoelectricity and its types

Piezoelectricity is the generation of an electrical charges in solid substances such as crystals, ceramics, and biological materials such as DNA, proteins, and so on. This phenomenon occurs when these materials are subjected to mechanical stress. The theory of piezoelectricity involves the production of electrical energy via by means of applied pressure and the presence of latent heat.

The piezoelectric effect in crystalline materials with no inversion symmetry arises from continuous electromechanical interactions of mechanical and electric states. Since this phenomenon is reversible, materials that show the piezoelectric effect also exhibit an inverse phenomenon as well. The inverse piezoelectric effect involves the internal development of mechanical pressure when an electric field is applied. PZT crystals, For instance, when deformed by approximately one percent of their original dimension, they result in observable piezoelectric energy. Conversely, applying an electric field to these materials causes them to shift around 0.1% of their static dimension, making use of the inverse piezoelectric effect to generate ultrasonic waves.

This effect was discovered in 1880 by Jacques and Pierre Curie. Since then, the piezoelectric effect has found various practical applications. Sound generation and monitoring, piezo printing with ink jets, high-voltage power generation, clock output in electronic components, microbalances, driving ultrasonic nozzles, and precise focusing of optical assembly are examples.

#### 1.1.1 Mechanism in piezoelectric materials:

The occurrence of electrical bipole moments in materials is intimately related to the characteristics of the piezoelectric phenomenon. This effect can occur in crystals when ions occupy attice sites with asymmetric charge distributions (as observed in materials like KNN, BaTiO3, and PZTs), or it can be carried by molecular groups directly (as seen in cane sugar). The density or polarisation of dipoles in crystals may be calculated by adding the dipole moments per volume of the crystalline unit cell. The dipole density P indicates a vector field as dipole is a vector. Proximity between dipoles leads to their alignment within regions known as Weiss domains. Although these domains typically exhibit random orientations, they can be aligned through a process called poling, which entails putting a strong electric field through the material, usually at elevated temperatures. However, not all piezoelectric substances can be poled.

The shift in polarisation resulting from mechanical pressure is critical in the piezoelectric phenomena. This shift may occur as a result of environment rearrangement producing dipoles or reorientation of molecule dipole moment produced by external stress. Piezoelectricity, therefore, involves alterations in the strength, direction, or both aspects of polarization. The specific changes depend on:

- the aligning of P in the crystal;
- crystallographic symmetry;
- the applied mechanical pressure.

Variations in P result in variations in surface charge density on the crystal faces, as a result of the changing dipole density in the whole substance, the electric field propagating between opposite ends changes.

#### **Piezoelectric effect types:**

#### • Direct Piezoelectric effect:-

It is due to change in the electric polarisation of a substance caused by mechanical pressure. Electrical polarisation is the shift in positive and negative charges that produces a peripheral electric field. The applied force in the material causes the creation of potential differences. This phenomenon is known as the direct piezoelectric effect. Composite materials with high piezoelectric effects, such as lead zirconate titanate and lithium niobate, are the greatest examples.

#### • Converse Piezoelectric effect:-

The reverse piezoelectric effect happens when the piezoelectric effect is reversed. This may be created by using electrical energy to cause a crystal to grow. This effect's primary role is to transform electrical energy into mechanical energy.

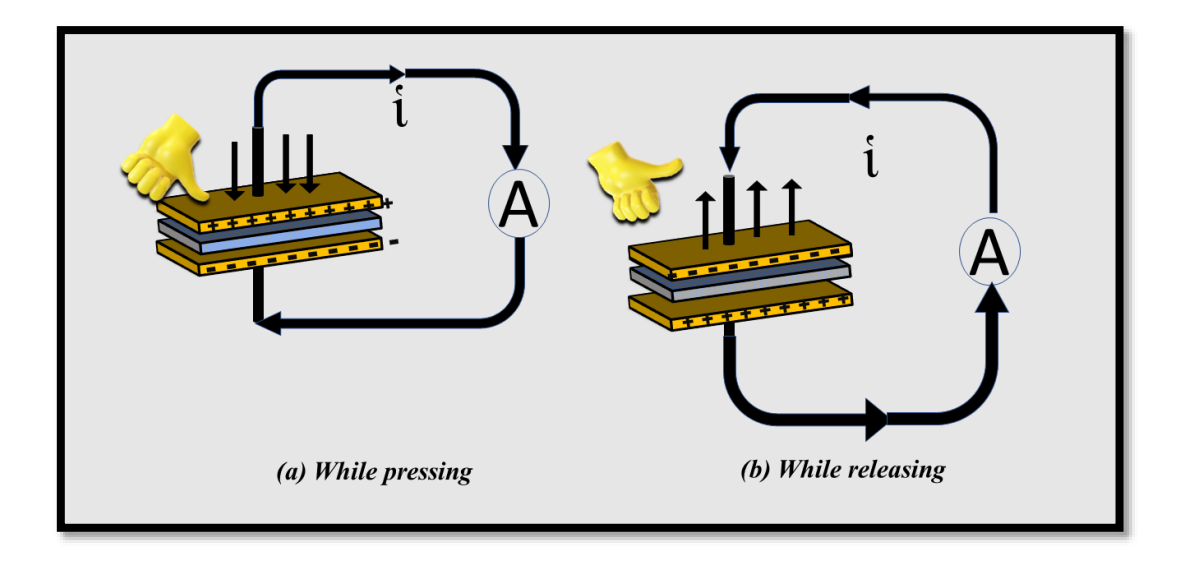


Fig. 1.1. (a) Working process for direct piezoelectric phenomena while pressing (b) Working process for converse piezoelectric phenomena while releasing

#### 1.2 Piezoelectric materials and their types

Piezoelectric materials (PMs) can be classified into three main types: crystalline, ceramic, and polymeric. Common examples of piezoelectric ceramics include lead zirconate titanate (PZT), BaTiO<sub>3</sub>, and lead titanate. GaN and ZnO, despite having larger band gaps, can also be considered ceramics. Synthetic ceramics PM's have beneficial over single crystals, as they can be easily produced in various forms and sizes without constraints related to crystallography. Organic polymer PMs, such as PVDF, have a lower Y comparing with inorganic PMs. Piezoelectric polymers, like PVDF with a piezoelectric stress constant (g<sub>33</sub>) of 240 mV-m/N, demonstrate higher values than ceramics like PZT with a g<sub>33</sub> of 11 mV-m/N. This characteristic makes piezoelectric polymers suitable for sensor applications, where the g<sub>33</sub> value is an important metric.

#### PIEZOELECTRIC MATERIALS AND IT'S TYPES

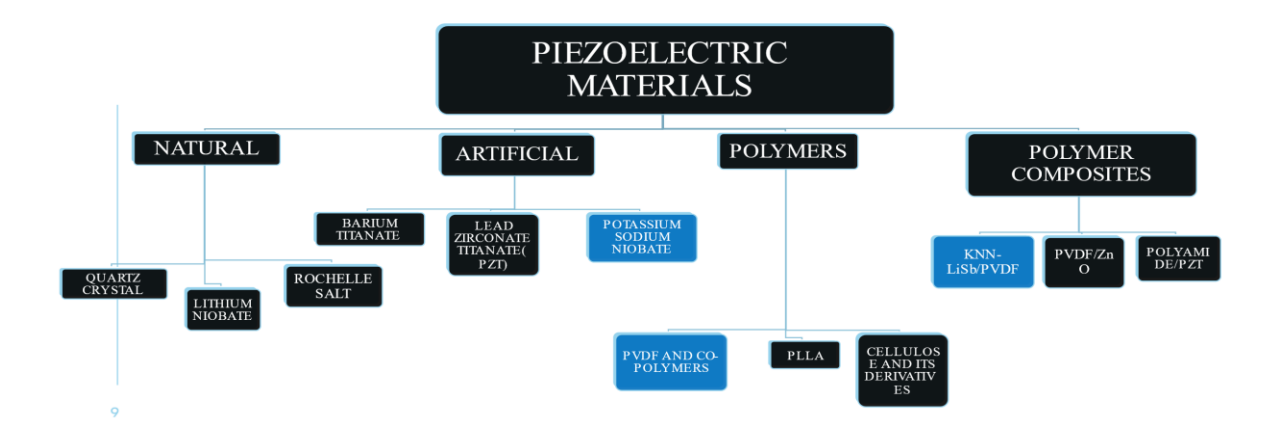


Fig. 1.2. Piezoelectric materials and their types

## 1.3 Applications of Piezoelectric Materials:

In modern times, electrical devices go beyond simple electrical connections and incorporate piezoelectricity as a common feature across various applications. Piezoelectricity finds

application in numerous sectors like medical, electronics etc . The progress in the advancement of artificial piezo materials, such as piezo-ceramics, has led to their widespread use in several sectors. These applications include:

- Piezoelectric Motors
- Energy harvesters
- Actuators
- Sensors
- Piezoelectric buzzers
- Instrument pickups
- Microphones
- Nano-positioning in AFM (Atomic Force Microscopy) and STM (Scanning Tunneling Microscopy)

The utilization of piezoelectricity in these various fields highlights its significance and versatility in modern-day electrical devices.

## 2. Experimental section

#### 2.1 Material and method used:-

Potassium Carbonate (K<sub>2</sub>CO<sub>3</sub>, 99%), Sodium Carbonate (Na<sub>2</sub>CO<sub>3</sub>, 98%), Niobium pentaoxide (Nb<sub>2</sub>O<sub>5</sub>, 99.5%), Lithium Carbonate (Li<sub>2</sub>CO<sub>3</sub>,99%), Antimony pentaoxide(Sb<sub>2</sub>O<sub>5</sub>,99%) and propanol (C<sub>3</sub>H<sub>8</sub>O) were purchased from Alfa-Aesar, India. The chemicals mentioned were utilized in the synthesis of pure KNN-LiSb and were used in their original form without undergoing additional purification.

#### The Solid State Reaction Method:-

Solid-state synthesis, often known as the ceramic method, involves a chemical method resulting in the creation of a fresh solid substance with an established framework from solid initial ingredients. The final products obtained from this process find wide application in the fields of energy and electrical systems, encompassing polycrystalline materials, single crystals, glasses, and thin-film materials.

In the solid-state process, fine-grain metallic mixtures are thoroughly blended, shaped into pellets, and subjected to specific temperatures for a designated duration. Many metallic compounds, for instance metallic oxides alongside salts, necessitate severe surroundings, such as extreme pressure and temperature, in order to begin processes in either a melted flux or a quickly condensed vapour phase.

The assessment of the reaction rate in solid-state process holds paramount importance. Due to the limited means of purifying the resulting solids, solid-state reactions must reach completion. The reaction rate in solid-state synthesis is influenced by various factors, includes the structure characteristics, arrangement and, the rate of diffusion, and the thermodynamic aspects associating with nucleations and reactions. The chemical precursors and preparation techniques

employed play a significant role in determining the chemical and physical characteristics of the ultimate products.

#### 2.2 Synthesis of KNN-LiSb ceramic powder:-

Lead-free (KNN-LiSb) ceramics were prepared through the conventional solid-state reaction technique. The raw materials employed in this synthesis included Potassium Carbonate, Sodium Carbonate, Niobium Pentoxide doped with lithium carbonate, and Antimony Pentoxide. These materials were initially combined in stoichiometric amounts and mixed in a Jar roller mill with steel balls for a period of 24 hours, utilizing propanol as the medium. The synthesis aimed to obtain 10 grams of KNN-LiSb ceramic powder, following the reaction presented below:

$$0.228 \; K_2CO_3 \; + \; 0.247 Nb_2CO_3 \; + \; 0.025 Li_2CO_3 + 0.025 Sb_2O_5 + 0.475 Nb_2O_5 \\ \\ [0.95(K_{0.48}Na_{0.52})NbO_3 + 0.05 LiSbO_3] \; + \; 0.5 \; CO_2 \; \uparrow$$

The KNN-LiSb powder was separated from the propanol by employing filter paper. Subsequently, the thoroughly mixed powder mixture underwent drying at 65 °C in an oven for a duration of 3-4 hours. To obtain a fine powder consistency, the dried powder was manually ground using a mortar and pestle for approximately 6-7 hours. Finally, the dried powder was subjected to calcination in ambient air for 4 hours, with temperature intervals of 850 °C, 900 °C, and 950 °C. The temperature profile specified the temperature of 900° C as the key point in the calcination process.

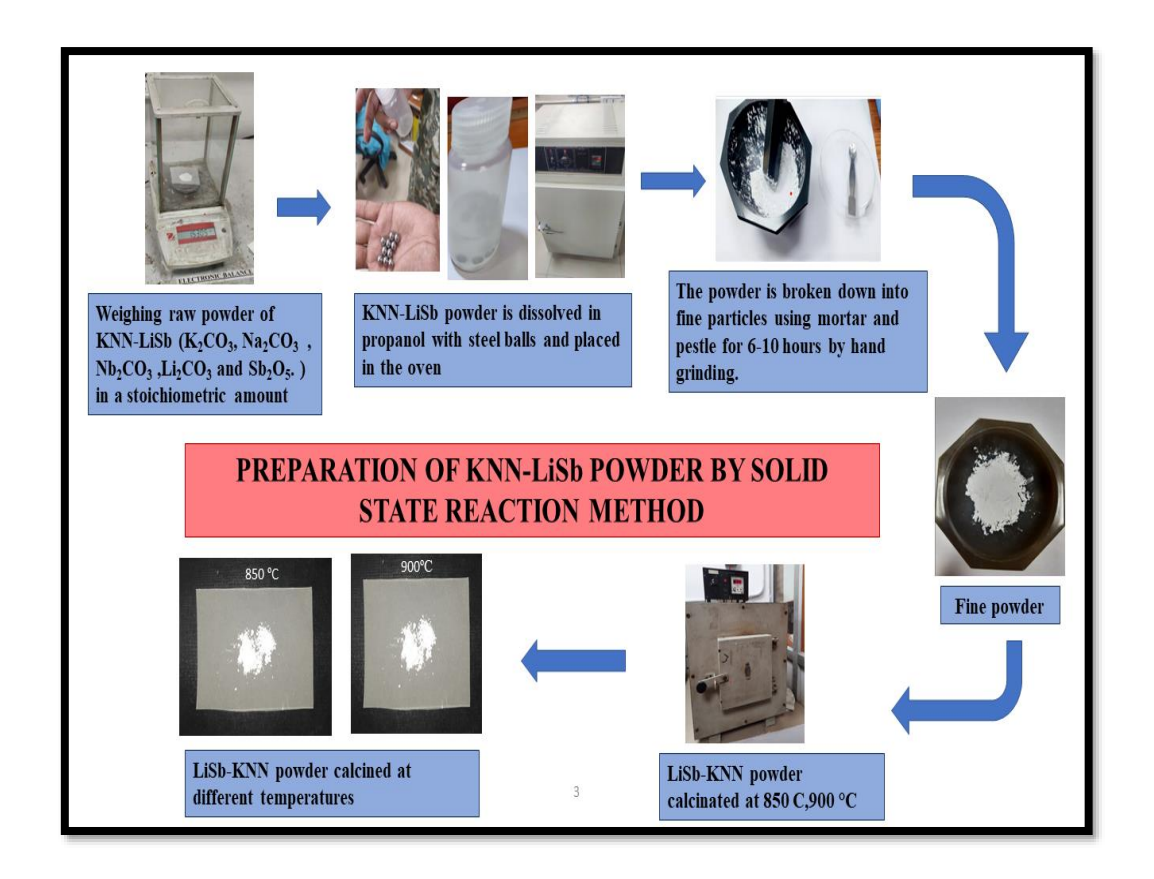


Fig. 2.1. Systematic illustration of KNN-LiSb powder synthesis by solid-state reaction method.

The reason behind choosing KNN-LiSb ceramic as filler material in polymer:-

- high dielectric constant.
- High curie temperature.
- Cost-effective.
- Lead-free and environment-friendly.
- Good piezoelectric properties.
- Excellent potential for the future.

## 2.3 Synthesis of KNN-LiSb /PVDF composite film.

PVDF and DMF was bought from Alfa Aesar Material Company. To create a homogenous, clear solution, PVDF powder was mixed in (N, N)-Dimethylformamide by stirring within a magnetic stirrer at 50°C for 1 hour. KNN-LiSb particles that had been calcined were added to DMF at changing concentrations — 0%, 5%, 10%, 15%, and 20% on the weight of the polymer and ultrasonically processed for 30 minutes at room temperature. To reduce particle agglomeration, the produced KNN-LiSb solutions were afterward fused in a PVDF mixture and stirred by a magnetic stirrer at 50°C for 4 hours. This mixture was then subjected to a 15-minute ultrasonication in the ultrasonic cleaner. The homogeneous solution was placed onto a glass substrate and dried for an hour at 80 °C for producing flexible KNN-LiSb /PVDF films. Finally, the film was easily detached from the glass substrate by peeling it off. The entire composite film extraction technique was carried out in an air-conditioned setting. Fig. 2.2 depicts a schematic representation of the fabrication process of KNN-LiSb/PVDF flexible composite film.

The reason behind choosing POLYVINYLIDENE FLUORIDE (PVDF) polymer as a matrix:-

- It is a semi-crystalline polymer having five phases of a crystalline area like  $\alpha$ ,  $\beta$ ,  $\gamma$ ,  $\delta$ ,  $\epsilon$ .
- Highly crystalline β-phase of PVDF is well known for its piezoelectric properties.
- PVDF is well known for good flexibility and mechanical integrity.
- It is cost-effective and light in weight.
- PVDF has a higher piezoelectric coefficient than other polymeric materials like nylon-11, polypropylene, polydimethylsiloxane, etc.
- A variety of methods including mechanical stretching, the introduction of different filler materials into PVDF material, and the electrospinning process, have been utilized to transition from the alpha phase to the beta phase.

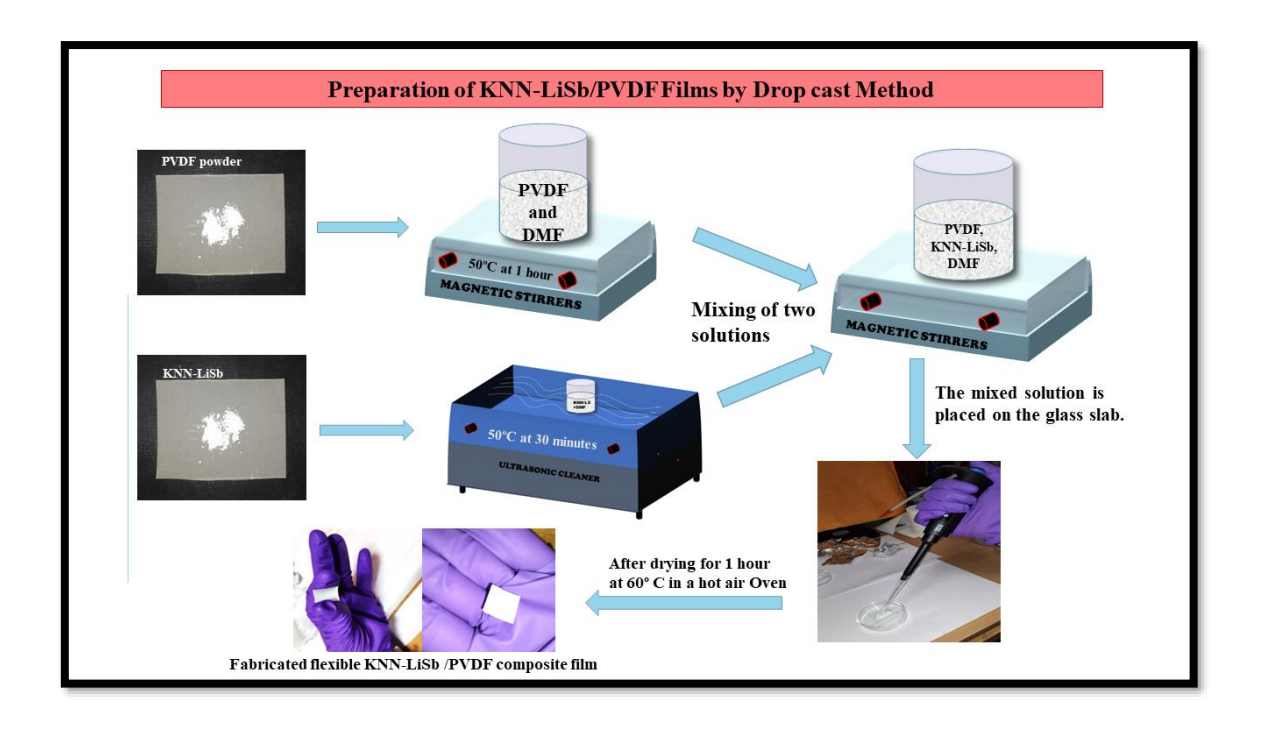


Fig. 2.2. Schematic representation of fabrication process of KNN-LiSb/PVDF flexible composite film.

#### **Drop Cast Method:**

Drop casting is a simple film-forming process that is employed by many research organizations since it requires no special equipment. Following the evaporation of the solvent, the solution containing the required material is cast on a substrate. However, getting a homogeneous layer and controlling its thickness (both of which are critical for producing functional OPV devices) is challenging [6,8]. This process is similar to spin coating. Additionally, the thickness and properties of the film are influenced by the volume and concentration of the dispersion. The structure of the film is also affected by factors such as substrate wetness, evaporation rate, and drying duration. It is often advised to use volatile solvents that can adequately wet the substrate during this process. Spin coating offers the advantage of minimizing material wastage.

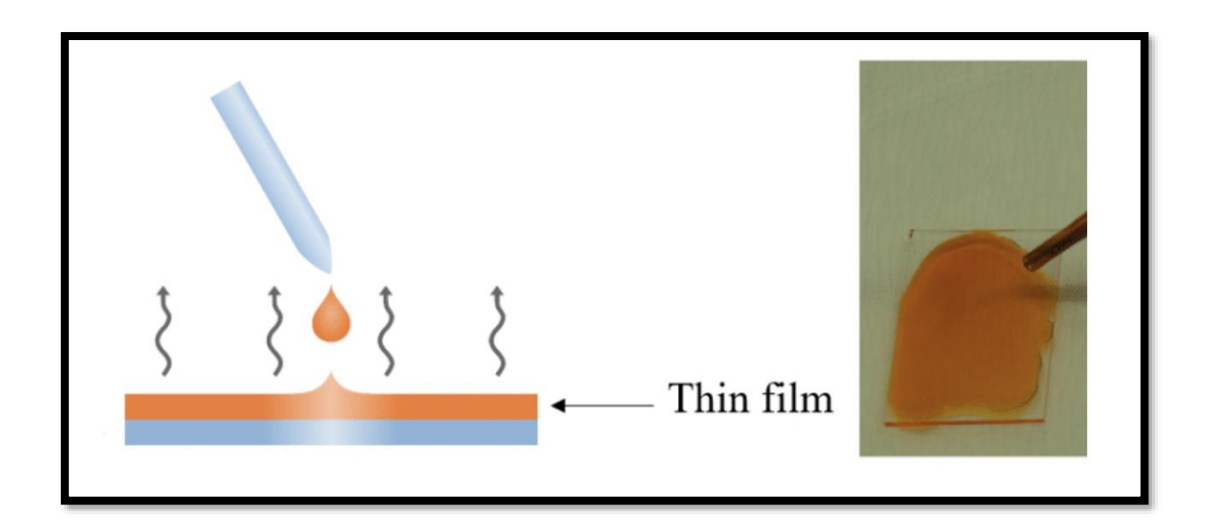


Fig. 2.3. Pictorial representation of thin film formation by Drop Cast Method

## 2.4 Creation of a piezoelectric generator based on KNN-LiSb /PVDF (PEG)

For the construction of PEG, the pliable KNN-LiSb/PVDF films have been created and sliced into 1.4\*1.4 cm² pieces, which were then taped with aluminum to construct the upper and lower electrode of PEG. The resultant signals when connected to the exterior circuit were then measured after the copper cables were joined to the aluminum foil using a silvery paste. Fig. 2.4 depicts the circuit illustration of the constructed Piezoelectric generator apparatus.

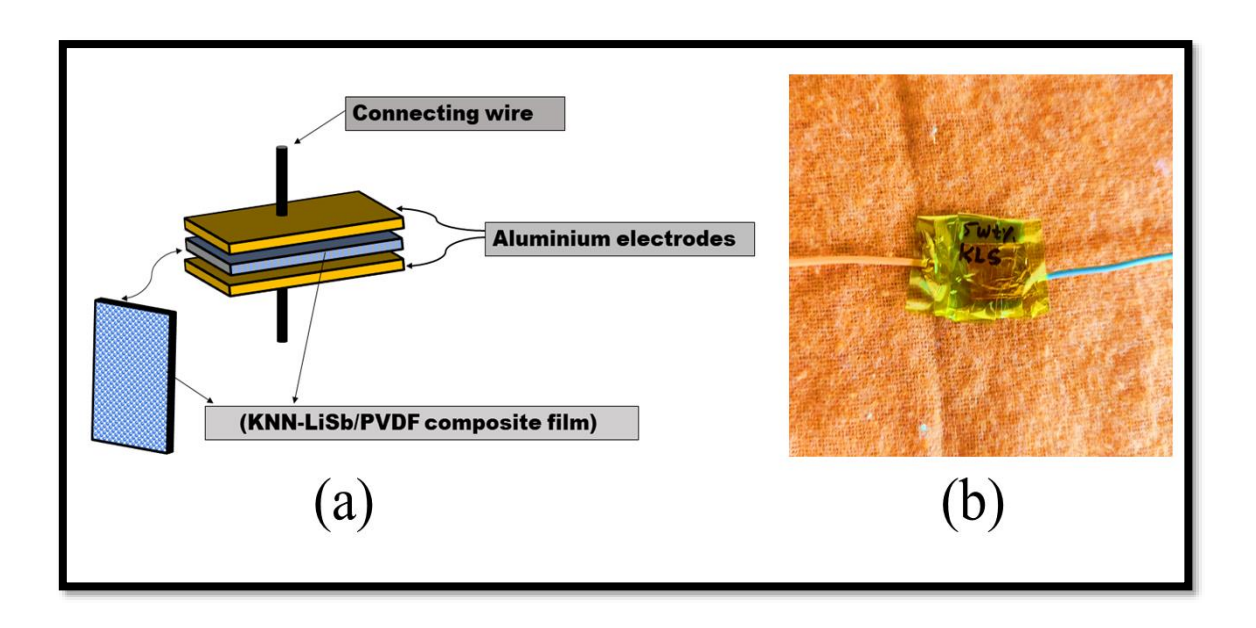


Fig. 2.4. (a) Illustrative diagram of the constructed Piezo Electric Generator apparatus. (b) image of constructed Piezoelectric generator device.

#### 2.5 Characterization Techniques:-



Fig. 2.5. (Cu-Karadiation,  $\lambda$ = 1.5406 Å, Make Bruker, Model: D8 Discover).

The crystal lattice arrangement of the produced KNN-LiSb powder and composite films was highlighted by X-Ray Analysis (XRD; Rigaku, Ultima - IV) with a Cu- $K_{\alpha}$  radiative source (1.54Å). Additionally, Rietveld refinement was performed using Fullprof Software to obtain refined cell parameters for the calcined and sintered KNN-LiSb samples. The origin of the  $\beta$ -phase in KNN-LiSb/PVDF-based films was analyzed under FTIR analysis. (PerkinElmer FTIR spectrum-II). Furthermore, the produced resultant voltages and short-circuiting current of the constructed Piezo Electric Generator devices were measured with the help of DSO (Digital Storage Oscilloscope) (Tektronix, MDO500) plus a digital current and voltmeter (Keithley DMM7510).

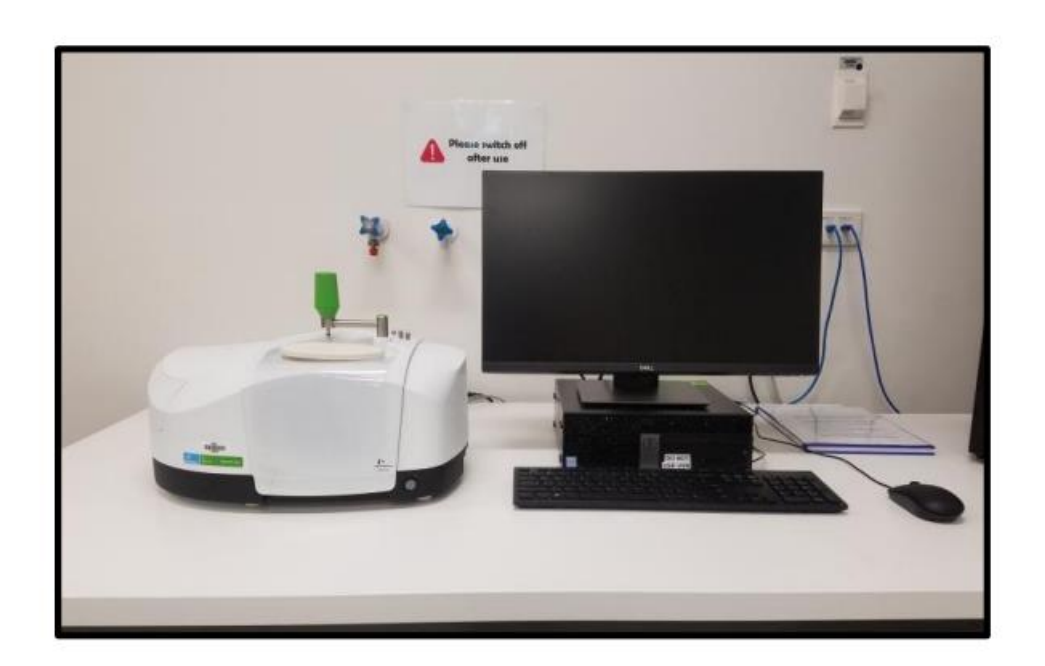


Fig. 2.6. Photograph of Perkin Elmer Two–Spectrum FTIR spectrometers

#### 3. Result and Discussion

#### 3.1 XRD Plot and analysis of prepared KNN-LiSb powder:-

To gain a comprehensive an in-depth knowledge of phase development and find the optimal calcination temperature for KNNLiSb powder, calcination was carried out at temperatures ranging from 850-950 °C. The provided plot illustrates are room temperature powder XRD patterns recorded for KNNLiSb powder that underwent calcination at 900 °C. The diffraction patterns exhibit Bragg peaks corresponding to various crystallographic planes, namely (100), (111), (102), (022), (200), (122), (211), (131), (220), (040), (222), (300), (024), and (311), for all the calcined samples.

Of particular interest are the (022) and (200) peaks around 2θ = 45°-46.5°, which aid in determining the phase structures of KNN-based ceramics. The XRD plots clearly show a split peak, with the (022) diffraction peak displaying higher intensity compared to the (200) diffraction peak. This intensity difference suggests that the calcined ceramics adopt an orthorhombic phase [10-15]. The XRD data extracted is consistent with the standard JCPDS card no. 98-024-7572., confirming the orthorhombic structure of the KNNLiSb ceramic with the space group Amm2. Notably, no additional peaks were observed, indicating the successful synthesis of KNN ceramic powder through the solid-state reaction process.

Throughout all the calcination temperatures, peaks corresponding to the KNN-LiSb phase consistently appeared. However, the X-ray peaks became progressively narrower and sharper as the calcination temperature increased from 850 to 950 °C, indicating enhanced crystallinity, as anticipated.

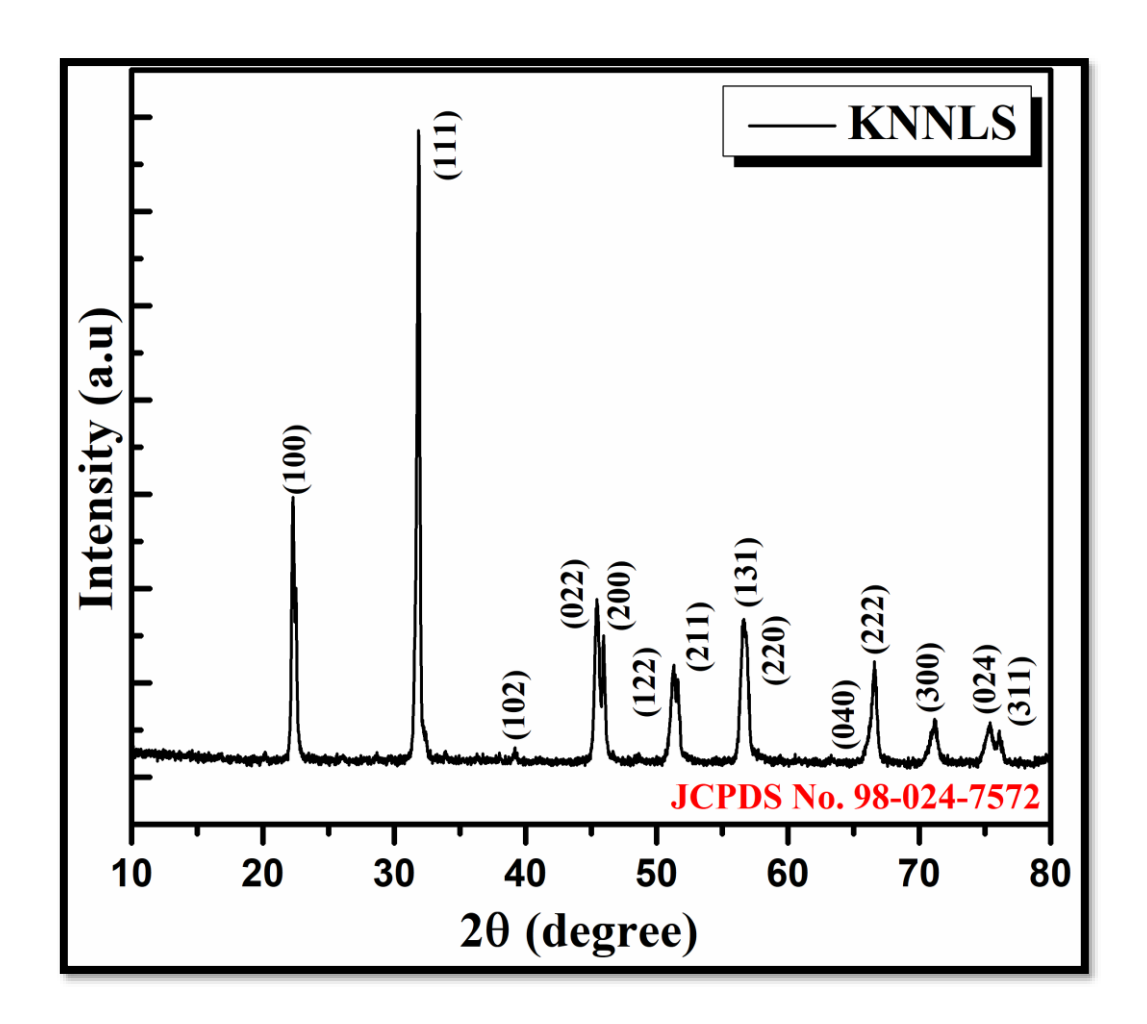


Fig. 3.1. XRD pattern of calcined KNN-LiSb powder

#### Rietveld Refinement plot and analysis of Prepared KNN-LiSb powder:-

The XRD data obtained from the calcination of KNN-LiSb ceramic powder at various temperatures was subjected to Rietveld refinement using Fullprof software. The matched XRD patterns generated by the software can be viewed in Figure 3.2, and the resulting structure and characteristic values are outlined in the table below. The crystalline structure analysis revealed that all the calcined powders exhibited a perfectly-matched orthorhombic phase.

Upon inspection of the table, it is evident that the sample calcined at 900 °C demonstrated the lowest value of goodness of fit ( $\chi^2$ ), indicating the reliability and rationality of the

refinement results for this particular sample. Specifically, the sample calcined at 900 °C exhibited attice constants of a = 3.9524 Å, b = 5.6328 Å, and c = 5.6591 Å. A calcination temperature of 900 °C was determined as the optimum temperature to produce KNN-LiSb ceramic powders based on XRD analysis and Rietveld refinement.. The acquired XRD data of the KNN-LiSb powder underwent Rietveld refinement using Fullprof software, and the corresponding matched XRD patterns can be seen in the table below. The resulting structure and characteristic values are provided, and it is noteworthy that the sample sintered at 900 °C displayed the lowest value of goodness of fit ( $\chi^2$ ).

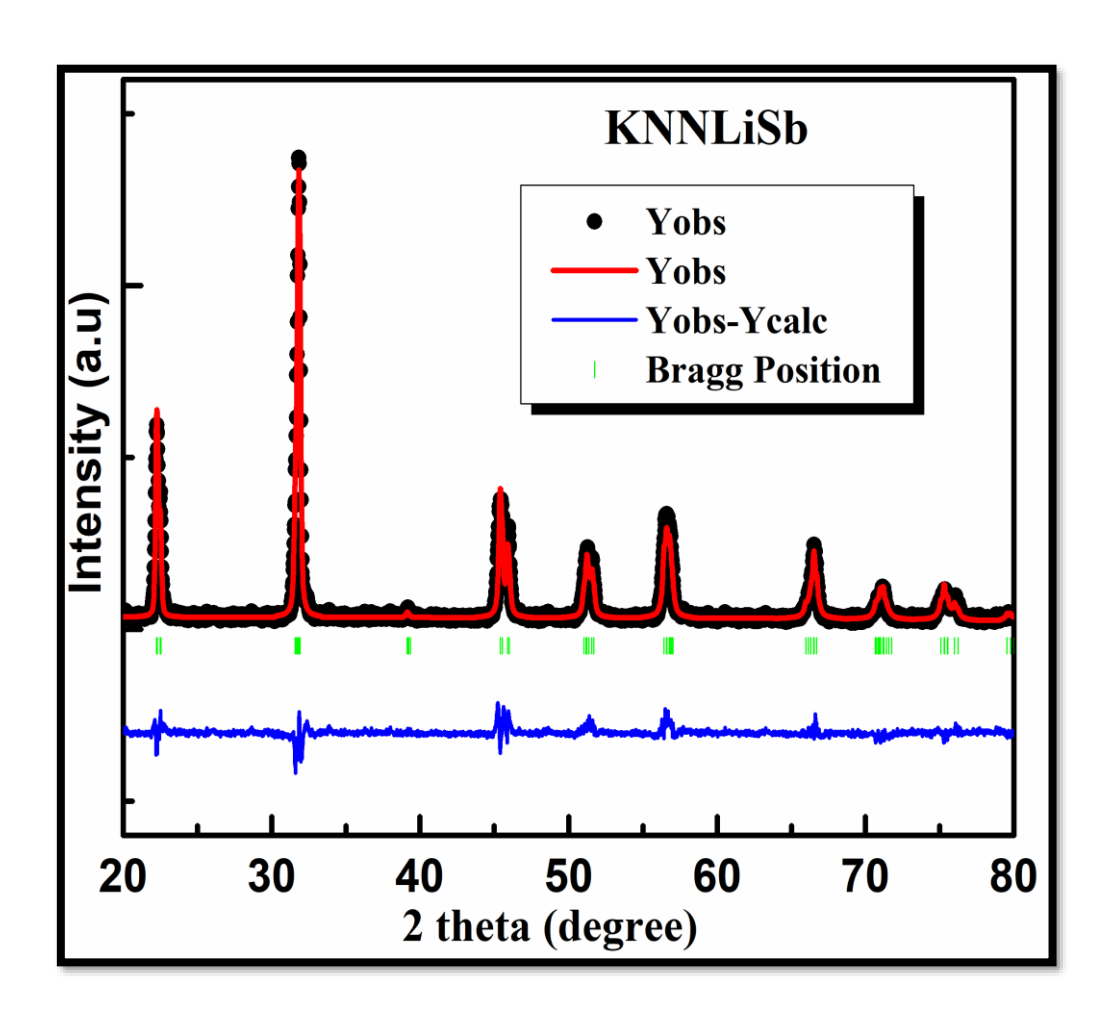


Fig. 3.2. Rietveld refinement of synthesized KNN-LiSb powder

S. No.	Parameter	Calcination Temperature (900° C)
		· ·
1.	Crystal System	Orthorhombic
2.	Direct Cell length, <i>a</i> (Å)	3.9524
3.	Direct Cell length, <i>b</i> (Å)	5.6328
4.	Direct Cell length, $c(\mathring{A})$	5.6591
5.	Direct Zell angle, $\alpha = \beta = \gamma(^{\circ})$	90
6.	Normal Volume, $V(\mathring{A}^3)$	125.9884
7.	Crystal System	Orthorhombic
8.	Reciprocal Cell length, $a^*(\mathring{A})$	0.2530
9.	Reciprocal Cell length, $b^*(\mathring{A})$	0.1775
10.	Reciprocal Cell length, $c*(\mathring{A})$	0.1767
11.	Reciprocal ell angle $\alpha^*=\beta^*=\gamma^*(^\circ)$	90
12.	Reciprocal Volume, $V^*(\mathring{A}^3)$	0.007937
13.	Space	Amm2
14.	Number of space groups	38
15.	$R_p$	24.8
16.	$R_{wp}$	23.4
17.	$R_e$	9.81
18.	$\chi^2$ (Goodness of fit)	5.680

Table 2. Various parameters were calculated using Rietveld refinement by Full Proof software.

# $3.2\ Morphology$ and micro-arrangement study of pure and KNN-LiSb /PVDF multilayered films

The produced films, comprising only PVDF and KNN-LiSb /PVDF flexible-produced films, underwent XRD analysis for evaluating their crystalline properties. The corresponding graphs

are shown in Fig. 3.3. The non-polar  $\alpha$ -phase of PVDF is thought to be responsible for the tiny and broad diffraction peak at ~18.2°, whereas the existence of a peak at ~20.1° in all manufactured films is thought to be a result of the polymer's polar-crystalline  $\beta$ - phase [41-47]. The greater intensity of the XRD peaks associated with the  $\beta$ -phase compared to the  $\alpha$ -phase as shown in Fig. 3.3 further supports the dominance of the  $\beta$ -phase on the  $\alpha$ -phase in all generated films. Furthermore, the XRD plots indicate that when the concentration of KNN-LiSb particles grows in the PVDF matrix, the magnitude of the diffraction peaks relating to the KNN-LiSb particles rises while the magnitude of the PVDF-associated peaks weakens.

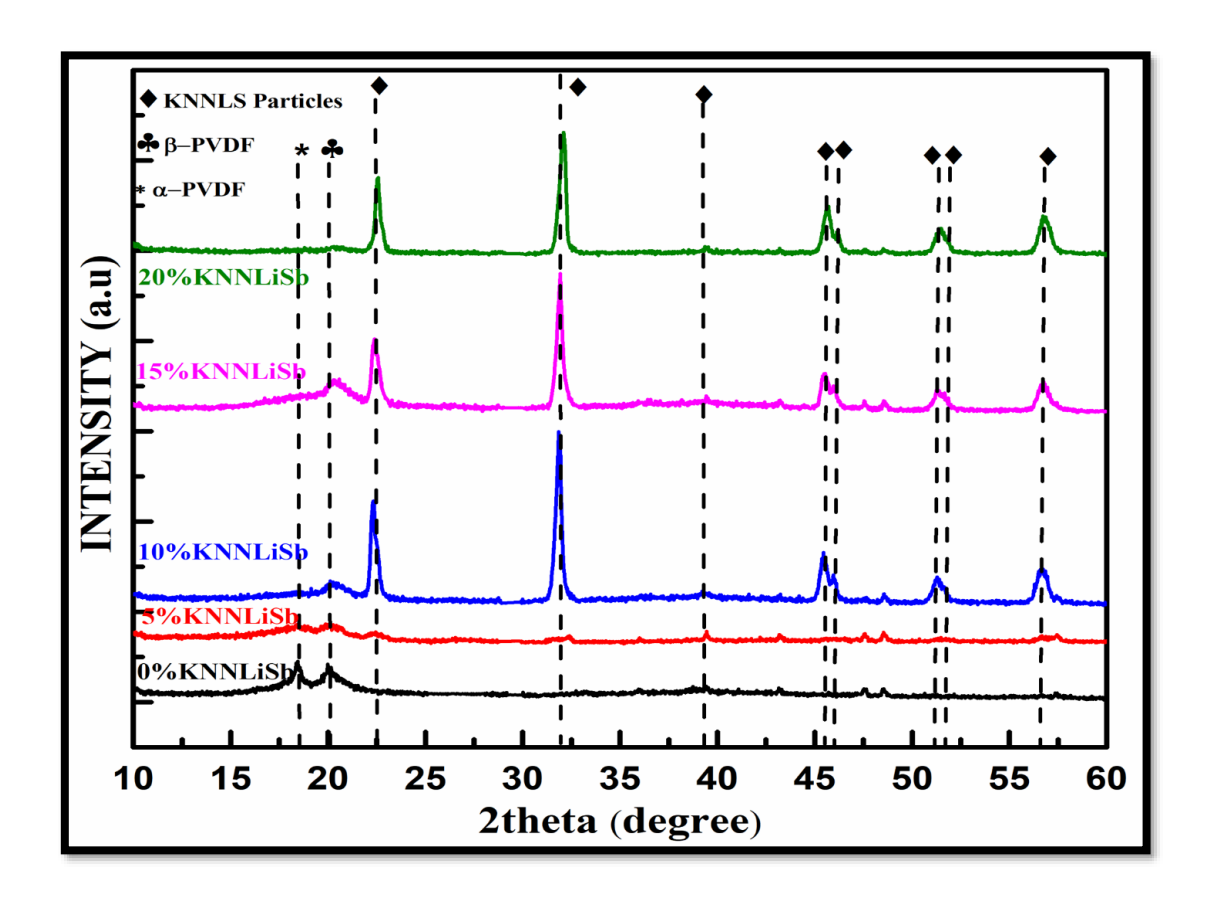


Fig. 3.3. XRD pattern of various content of KNN-LiSb /PVDF Composite Films.

SEM was employed to analyze the surface profile of the KNN-LiSb /PVDF-based composite film, and the resultant images are displayed in Fig. 3.4. The composite films of KNN-LiSb

/PVDF in Fig. 3.4 exhibit homogeneous distribution and KNN-LiSb produced particles inside the PVDF matrix.

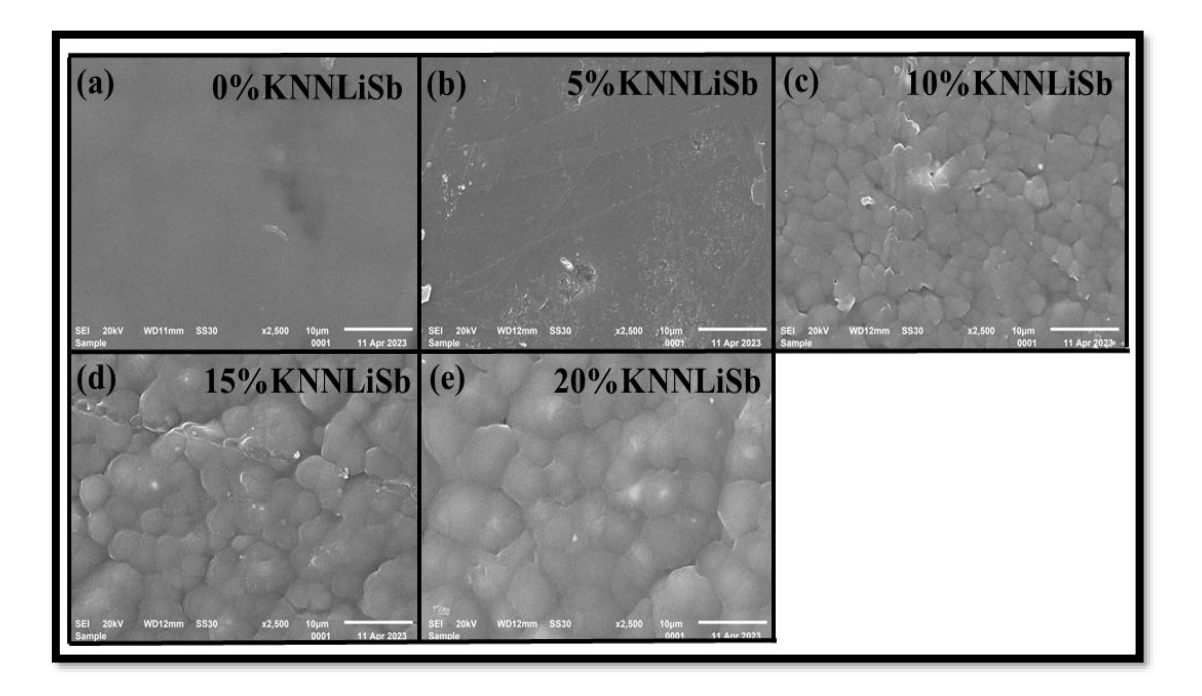


Fig. 3.4. (a-e) SEM surface morphology micrographs of KNN-LiSb /PVDF with varied concentrations of KNN-LiSb based powder in PVDF polymer on a 10μm scale.

## 3.3 Fourier Transform-Infrared Spectroscopy (FTIR) Studies

The FTIR study provided further insight into the influence of KNN-LiSb-based particles on the crystalline arrangement of PVDF in composite films. The FTIR spectrum in Fig. 3.5 confirmed the presence of both  $\alpha$  and  $\beta$  phases in every produced film. The characteristic tips of the  $\alpha$ -phase were identified at 765, 799, 978, and 1382 cm<sup>-1</sup>, while the characteristic tips of the  $\beta$ -phase are identified at 840, 876, 1071, 1172, 1234, and 1232 cm<sup>-1</sup> for the range 600 to 1500 cm<sup>-1</sup>. All of the KNN-LiSb /PVDF synthetic films had sharper  $\beta$ -phase absorbance peaks

than the pristine PVDF film, showing that the inclusion of KNN-LiSb -based powder encourages increased PVDF  $\beta$ -phase crystallization.

Furthermore, the absorbance peak at 840 cm<sup>-1</sup>, corresponding to the  $\beta$  phase of PVDF, increases as there is an increase in the concentration of KNN-LiSb ceramic in the PVDF polymer up to 15 % concentration, before decreasing. The sample with 15% KNN-LiSb content revealed the minimal absorbance magnitude for the PVDF  $\alpha$ -phase. The growth of the PVDF  $\beta$ -phase in the composite films with the presence of KNN-LiSb ceramic can significantly impact the energy conversion efficiency of the produced films.

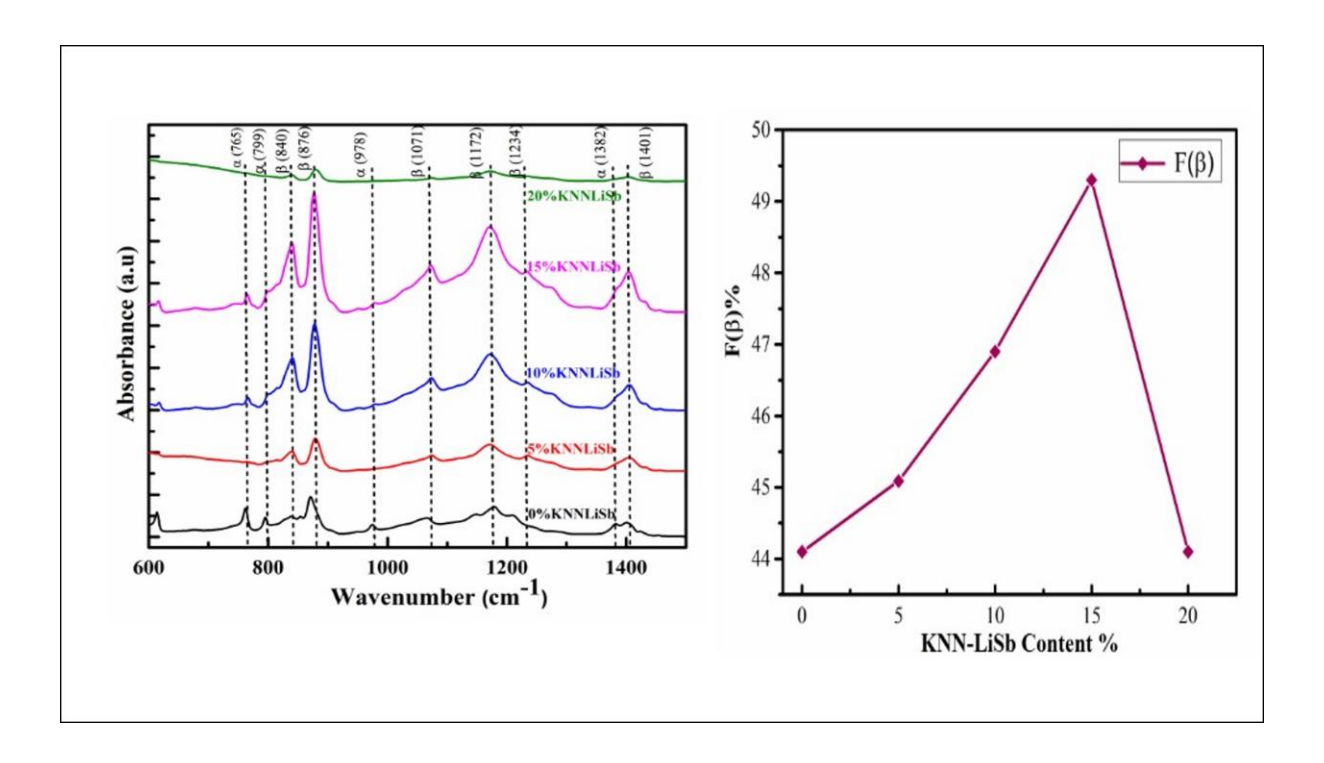


Fig. 3.5. (a) FTIR spectra of KNN-LiSb powder content in the PVDF polymer (b) Variation in  $F(\beta)$  as a function of KNN-LiSb powder content in PVDF polymer

#### 3.4 PEG device's piezoelectric performance

Fig. 3.6 depicts the constructed piezoelectric generating device's operation mechanism. Electric dipoles orient each other in one direction when a perpendicular force is exerted through the device, creating a potential difference between the two terminals. As a result, as shown in Fig. 3.6.(a) electrons travel via an external circuit from downward to upward therefore the current flows in opposite directions. The electric dipoles immediately reverse when the applied force on the device is released, causing the electron travels from upward to downward therefore current flows in the reverse direction as noticed in Fig. 3.6.(b). The resulting signals of this constructed PEG device were determined with an electrodynamic shaker on the device's surface. The Piezo-Electric Generator was linked to a device called a Digital Storage Oscilloscope for evaluating the open-circuitry voltage, and a digital multi-meter to assess the short-circuiting current. When pressure is applied on the device's surface, a potential difference develops along the generator, and the resultant voltage is observed on a computerized storing oscilloscope.

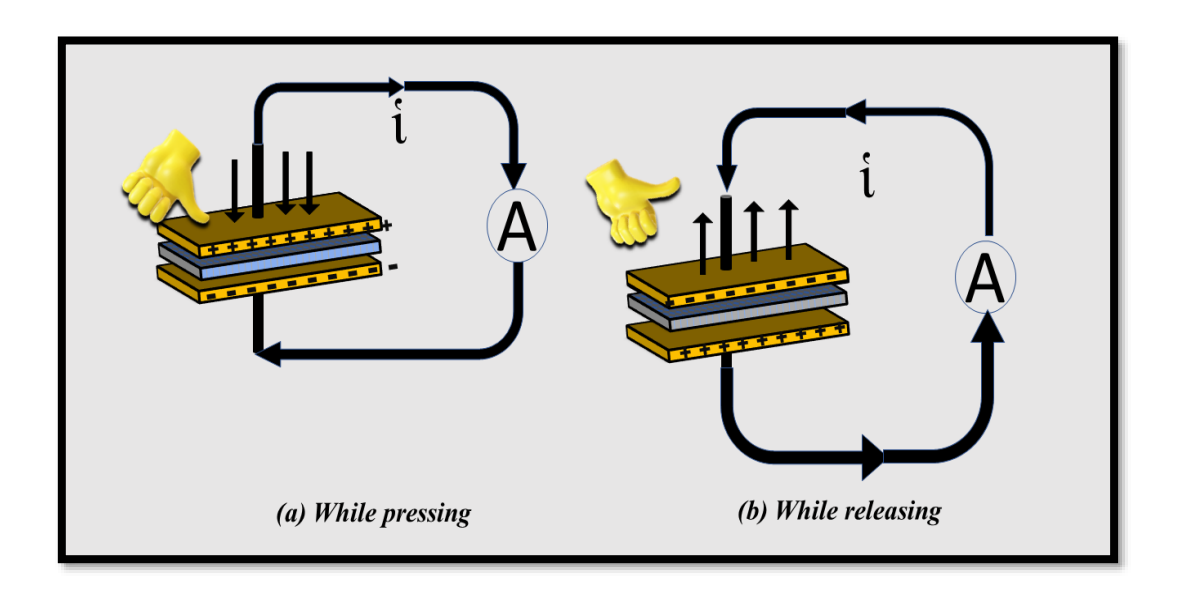


Fig. 3.6. (a) Working Mechanism PEG device while pressing (b) Working Mechanism PEG device while releasing

Plotting of the open-circuit voltage produced via the manufactured gadgets by the ready devices at various KNN-LiSb ceramic powder concentrations in the PVDF matrix at a frequency of 3 *Hz* [48-54] is displayed in Fig. 3.7. The fluctuation of the open-circuit voltage about KNN-LiSb ceramic particle concentration in the PVDF matrix is depicted in Fig. 3.7(f). The plot demonstrates that open-circuitry voltage initially increased with the rise in KNN-LiSb concentration in the PVDF matrix up to 15 % and then subsequently drops when KNN-LiSb content in the PVDF matrix rises to 20 %. The sample with 15 % KNN-LiSb particles had the greatest open-circuit voltage at 15.4 V. The produced open-circuitry voltages for unadultered PVDF, 5% KNN-LiSb, 10% KNN-LiSb, and 20% KNN-LiSb based PEGs are 5.19 V, 8.98 V, 9.12 V, and 13.82 V, respectively. Over 15% KNN-LiSb fillers are working within a Poly Vinylidene Fluoride matrix in an arrangement that restricts the formation of the PVDF phases and increases the likelihood of defects forming in the polymer matrix, which may be the cause of the observed drop in output voltage [46,47].

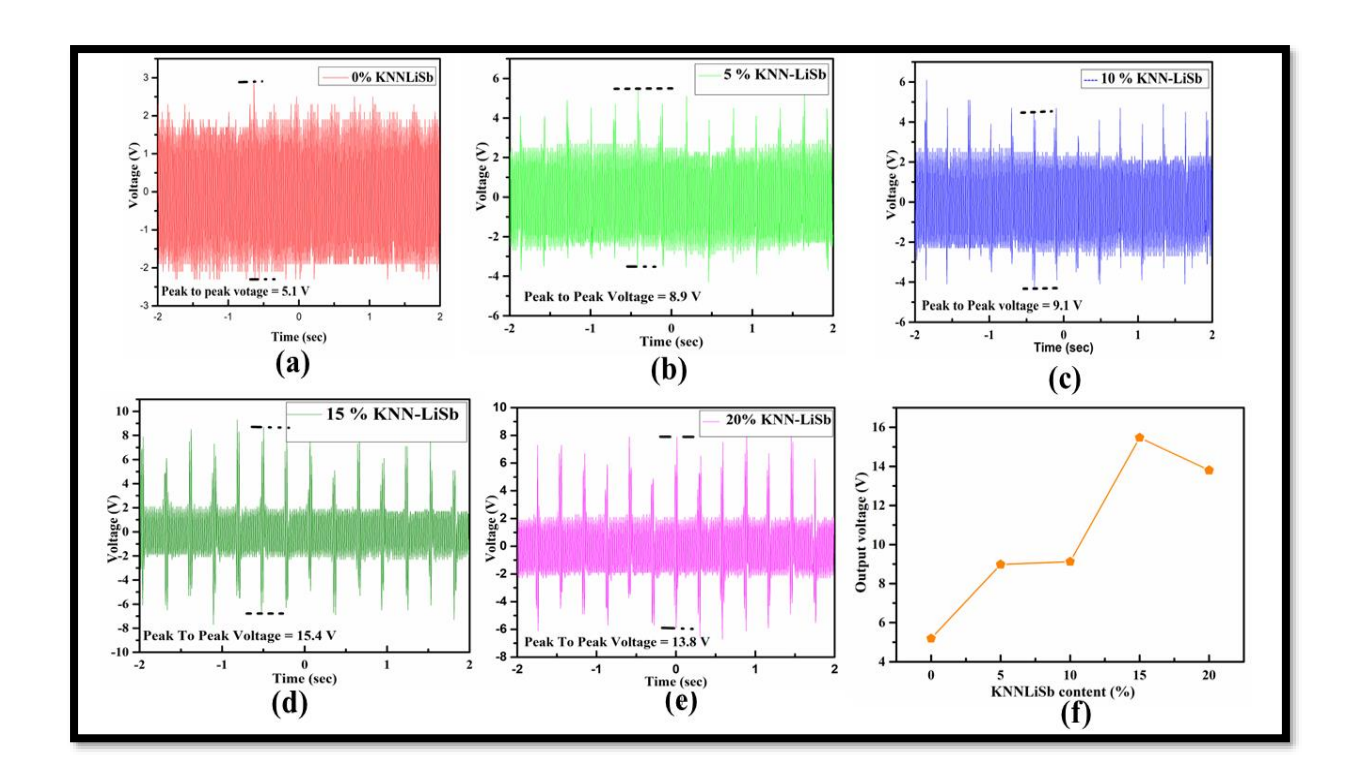


Fig. 3.7. (a-e) Open-circuitry voltage produced by a KNN-LiSb /PVDF PEG apparatus with varying KNN-LiSb based powder content within Poly Vinylidene Fluoride matrix and (f) Variability of open-circuitry current in PVDF matrix with change in KNN-LiSb concentration

SNO.	KNN-LiSb Content (wt. %)	F(β) ( in %)
1	0 (Pure PVDF)	44.1
2	5	45.09
3	10	46.9
4	15	49.3
5	20	44.1

Table 3.1 Variation of generated output oltage as a function of KNN-LiSb ceramic content in PVDF matrix.

The constructed devices' short circuit current was measured using the Electrodynamic Shaker. Fig. 3.8 shows comparable graphs. The short circuit current values for the samples containing 0%, 5%, 10%, 15%, and 20% KNN-LiSb powder in the PVDF matrix were 1.91μA, 1.95 μA, 2.05 μA, 2.14 μA, and 2.08 μA, respectively. The frequency range used for the measurements was 3 Hz to 4 Hz. Fig. 3.8(f) demonstrates how the amount of KNN-LiSb ceramic particles within a PVDF matrix affects the variation in short-circuit current. The Piezoelectric generator device with 15% KNN-LiSb within a PVDF matrix achieved the most significant short-circuiting current value. The mechanical reliability and longevity associated with 15% KNN-LiSb /PVDF PEG were tested under constant force ~1N.

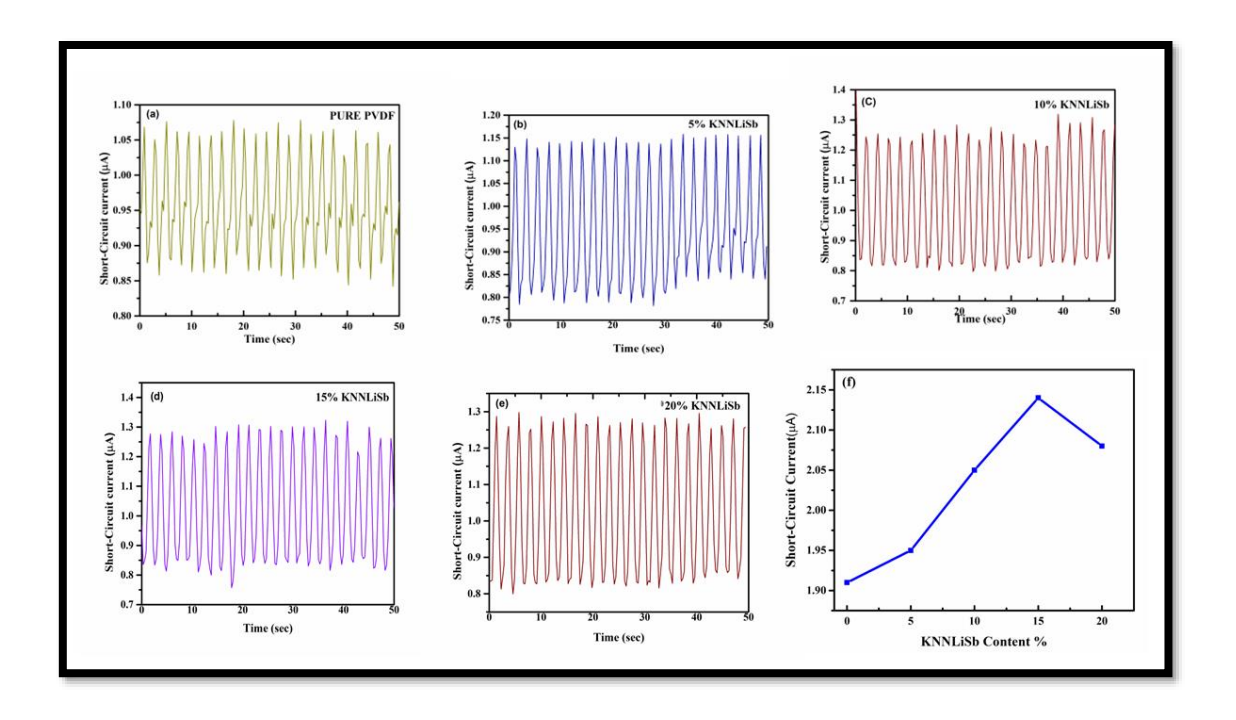


Fig. 3.8. (a-e) Short-circuiting current produced by a KNN-LiSb /PVDF PEG circuitry with varying KNN-LiSb powder content in the PVDF polymer and (f) Plot of short-circuiting current in PVDF matrix with of KNN-LiSb concentrations

SNO.	KNN-LiSb Content (wt. %)	Output current (μA)
1	0 (Pure PVDF)	1.91
2	5	1.95
3	10	2.05
4	15	2.14
5	20	2.08

Table 3.2 Variation of generated output urrent as a function of KNN-LiSb ceramic content in PVDF matrix.

#### 4. Conclusion:-

Finally, the researchers created an environmentally safe, Pb-free, flexible Piezo-Electric Energy Generator. They achieved this by utilizing a powdered version of KNN-LiSb as a filling agent within a polymer matrix. The X-Ray Diffractometry plot demonstrated that the PVDF βphase was present in all of the films prepared. Furthermore, FTIR analysis found that the mixing of KNN-LiSb particulates had significant impacts on the β-phase of Poly Vinylidene Fluoride. The use of KNN-LiSb powdered form as a filler agent within the Poly Vinylidene Fluoride matrix improved the PEG device's reaction or feedback. The maximum no-load voltage and short-circuiting current of the PVDF polymer PEG device are 15.47 V and 2.14μA, respectively. Furthermore, Circuitry was demonstrated to successfully collect energy by human body actions such as elbow bending, tap contracting, and so on. This study's synthesis technique proved to be practical and cost-effective, making it suitable for the production of large-scale, enhanced-performance ceramic-polymer multifunctional PEGs that are flexible, stable, and durable, and can be used in a variety of wearable and flexible powered electronics applications [56-58]. When creating a enhanced performance PEG, the choice of piezoelectric material is important. In this investigation, KNN-LiSb ceramic was mixed in polymer matrix. One downside of KNN-LiSb ceramics is that they have a high leakage current density, which restricts the PEG film's piezoelectric output responses [43-47]. Chemical doping, on the other hand, can increase the piezoelectric properties of KNN by raising its piezoelectric coefficient and stabilising its performance [46]. Substituting Nb<sup>5+</sup> ions in Potassium Sodium Niobate with Ta<sup>5+</sup>, Zi<sup>4+</sup>, Cu<sup>2+</sup>, Li<sup>+</sup>, and Sb<sup>5+</sup> ions, for example, might result in complex defects that restrict domain wall motion, minimise dielectric losses, and improve piezoelectric performance. Despite the fact that there have been few studies on employing modified KNN-LiSb in the polymer matrix to construct PEG, it is an area of research with significant potential to improve

the performance of PEG appliances [59]. As a result, In the future, there is significant potential for the advancement of PEG devices with enhanced piezoelectric performance. This progress can be achieved by incorporating chemically modified KNN-LiSb lead-free ceramic powder into PVDF (polyvinylidene fluoride) materials.

## 5. References:-

- [1] Alnajar, M. H., Sinha, N., & Kumar, B. (2022). Development of energy harvesting and ferroelectric characteristic of thulium-doped ZnO via graphene addition. *Materials Chemistry and Physics*, 292. https://doi.org/10.1016/J.MATCHEMPHYS.2022.126848
- [2] Badatya, S., Bharti, D. K., Srivastava, A. K., & Gupta, M. K. (2021). Solution-processed high-performance piezoelectric eggshell membrane PVDF layer composite nanogenerator via tuning the interfacial polarization. *Journal of Alloys and Compounds*, 863. https://doi.org/10.1016/j.jallcom.2020.158406
- [3] Batra, K., Sinha, N., Goel, S., Yadav, H., Joseph, A. J., & Kumar, B. (2018). Enhanced dielectric, ferroelectric and piezoelectric performance of Nd-ZnO nanorods and their application in flexible piezoelectric nanogenerator. *Journal of Alloys and Compounds*, 767, 1003–1011. <a href="https://doi.org/10.1016/J.JALLCOM.2018.07.187">https://doi.org/10.1016/J.JALLCOM.2018.07.187</a>
- [4] Bornand, V. (2015). Ferroelectric and dielectric properties in Li-doped ZnO nanorods.

  Thin Solid Films, 574, 152–155. https://doi.org/10.1016/J.TSF.2014.12.011
- [5] Chen, L., Wang, H., Zhao, P., Zhu, C., Cai, Z., Cen, Z., Li, L., & Wang, X. (2019).
  Multifunctional BaTiO 3 -(Bi 0.5 Na 0.5)TiO 3 -based MLCC with high-energy storage
  properties and temperature stability. *Journal of the American Ceramic Society*, 102(7),
  4178–4187. <a href="https://doi.org/10.1111/JACE.16292">https://doi.org/10.1111/JACE.16292</a>
- [6] Chen, X., Li, X., Shao, J., An, N., Tian, H., Wang, C., Han, T., Wang, L., & Lu, B. (2017). High-Performance Piezoelectric Nanogenerators with Imprinted P(VDF-TrFE)/BaTiO3 Nanocomposite Micropillars for Self-Powered Flexible Sensors. *Small*, 13(23). https://doi.org/10.1002/SMLL.201604245

- [7] Dong, H., Jian, J., Li, H., Jin, D., Chen, J., & Cheng, J. (2017). Improved dielectric tunability of PZT/BST multilayer thin films on Ti substrates. *Journal of Alloys and Compounds*, 725, 54–59. https://doi.org/10.1016/j.jallcom.2017.07.139
- [8] Du, H., Li, Z., Tang, F., Qu, S., Pei, Z., & Zhou, W. (2006). Preparation and piezoelectric properties of (K0.5Na0.5)NbO3 lead-free piezoelectric ceramics with pressure-less sintering. *Materials Science and Engineering B: Solid-State Materials for Advanced Technology*, 131(1–3), 83–87. <a href="https://doi.org/10.1016/j.mseb.2006.03.039">https://doi.org/10.1016/j.mseb.2006.03.039</a>
- [9] Ferreira, A., Silva, J., Sencadas, V., Ribelles, J. L. G., & Lanceros-Méndez, S. (2010). Poly[(vinylidene fluoride)-co-trifluoroethylene] membranes obtained by isothermal crystallization from solution. *Macromolecular Materials and Engineering*, 295(6), 523–528. <a href="https://doi.org/10.1002/MAME.201000020">https://doi.org/10.1002/MAME.201000020</a>
- [10] Goel, S., & Kumar, B. (2020a). A review on piezo-/ferro-electric properties of morphologically diverse ZnO nanostructures. *Journal of Alloys and Compounds*, 816, 152491. https://doi.org/10.1016/J.JALLCOM.2019.152491
- [11] Goel, S., & Kumar, B. (2020b). A review on piezo-/ferro-electric properties of morphologically diverse ZnO nanostructures. *Journal of Alloys and Compounds*, 816. <a href="https://doi.org/10.1016/j.jallcom.2019.152491">https://doi.org/10.1016/j.jallcom.2019.152491</a>
- [12] Goel, S., Sinha, N., Hussain, A., Joseph, A. J., Yadav, H., & Kumar, B. (2018). Sunset yellow dyed triglycine sulfate single crystals: enhanced thermal, mechanical, optical and di-/piezo-/ferro-/pyro-electric properties. *Journal of Materials Science: Materials in Electronics*, 29(16), 13449–13463. https://doi.org/10.1007/S10854-018-9470-9
- [13] Goel, S., Sinha, N., Yadav, H., Joseph, A. J., & Kumar, B. (2017a). Experimental investigation on the structural, dielectric, ferroelectric and piezoelectric properties of La doped ZnO nanoparticles and their application in dye-sensitized solar cells. *Physica E:*

- Low-Dimensional Systems and Nanostructures, 91, 72–81. https://doi.org/10.1016/j.physe.2017.04.010
- [14] Goel, S., Sinha, N., Yadav, H., Joseph, A. J., & Kumar, B. (2017b). Experimental investigation on the structural, dielectric, ferroelectric and piezoelectric properties of La doped ZnO nanoparticles and their application in dye-sensitized solar cells. *Physica E: Low-Dimensional Systems and Nanostructures*, 91, 72–81. <a href="https://doi.org/10.1016/J.PHYSE.2017.04.010">https://doi.org/10.1016/J.PHYSE.2017.04.010</a>
- [15] Hu, L., Zhang, G., Zhang, Y., Zhang, W., Wang, H., Liu, K., Zhang, Y., Li, Q., Chen, Y., & Shen, M. (2023). Enhanced pyroelectric properties of BNT-xBNN lead-free ferroelectric ceramics for energy harvesting. *Journal of Alloys and Compounds*, 169621. https://doi.org/10.1016/j.jallcom.2023.169621
- [16] Hu, P., Yan, L., Zhao, C., Zhang, Y., & Niu, J. (2018a). Double-layer structured PVDF nanocomposite film designed for flexible nanogenerator exhibiting enhanced piezoelectric output and mechanical property. *Composites Science and Technology*, 168, 327–335. https://doi.org/10.1016/J.COMPSCITECH.2018.10.021
- [17] Hu, P., Yan, L., Zhao, C., Zhang, Y., & Niu, J. (2018b). Double-layer structured PVDF nanocomposite film designed for flexible nanogenerator exhibiting enhanced piezoelectric output and mechanical property. *Composites Science and Technology*, 168, 327–335. https://doi.org/10.1016/j.compscitech.2018.10.021
- [18] Hussain, A., Sinha, N., Goel, S., Joseph, A. J., & Kumar, B. (2019). Y3+ doped 0.64PMN-0.36PT ceramic for energy scavenging applications: Excellent piezo-/ferroresponse with the investigations of true-remanent polarization and resistive leakage.

  \*Journal of Alloys and Compounds, 790, 274–287.\*

  https://doi.org/10.1016/j.jallcom.2019.03.144

- [19] Hyeon, D. Y., Lee, G. J., Lee, S. H., Park, J. J., Kim, S., Lee, M. K., & Park, K. Il. (2022a). High-temperature workable flexible piezoelectric energy harvester comprising thermally stable (K,Na)NbO3-based ceramic and polyimide composites. *Composites Part B: Engineering*, 234. https://doi.org/10.1016/j.compositesb.2022.109671
- [20] Hyeon, D. Y., Lee, G. J., Lee, S. H., Park, J. J., Kim, S., Lee, M. K., & Park, K. Il. (2022b). High-temperature workable flexible piezoelectric energy harvester comprising thermally stable (K,Na)NbO3-based ceramic and polyimide composites. *Composites Part B: Engineering*, 234, 109671. <a href="https://doi.org/10.1016/J.COMPOSITESB.2022.109671">https://doi.org/10.1016/J.COMPOSITESB.2022.109671</a>
- [21] Jeyaraman, A. R., Balasingam, S. K., Lee, C., Lee, H., Balakrishnan, B., Manickam, S., Yi, M., Kim, H. J., Sivalingam Nallathambi, K., Jun, Y., & Kuzhandaivel, H. (2019). Enhanced solar to electrical energy conversion of titania nanoparticles and nanotubes-based combined photoanodes for dye-sensitized solar cells. *Materials Letters*, 243, 180–182. <a href="https://doi.org/10.1016/J.MATLET.2019.02.006">https://doi.org/10.1016/J.MATLET.2019.02.006</a>
- [22] Jiten, C., Gaur, R., Laishram, R., & Singh, K. C. (2016). Effect of sintering temperature on the microstructural, dielectric, ferroelectric and piezoelectric properties of (Na0.5K0.5)NbO3 ceramics prepared from nanoscale powders. *Ceramics International*, 42(12), 14135–14140. https://doi.org/10.1016/j.ceramint.2016.06.029
- [23] Kang, H. B., Han, C. S., Pyun, J. C., Ryu, W. H., Kang, C. Y., & Cho, Y. S. (2015).
  (Na,K)NbO3 nanoparticle-embedded piezoelectric nanofiber composites for flexible nanogenerators. *Composites Science and Technology*, 111, 1–8.
  <a href="https://doi.org/10.1016/j.compscitech.2015.02.015">https://doi.org/10.1016/j.compscitech.2015.02.015</a>
- [24] Kang, L., An, H. L., Park, J. Y., Hong, M. H., Nahm, S., & Lee, C. G. (2019). La-doped p-type ZnO nanowire with enhanced piezoelectric performance for flexible

- nanogenerators. *Applied Surface Science*, 475, 969–973. https://doi.org/10.1016/J.APSUSC.2019.01.025
- [25] Kang, P. G., Yun, B. K., Sung, K. D., Lee, T. K., Lee, M., Lee, N., Oh, S. H., Jo, W., Seog, H. J., Ahn, C. W., Kim, I. W., & Jung, J. H. (2014). Piezoelectric power generation of vertically aligned lead-free (K,Na)NbO3 nanorod arrays. *RSC Advances*, 4(56), 29799–29805. https://doi.org/10.1039/C4RA02921F
- [26] Kaur, J., & Singh, H. (2020). Fabrication and analysis of piezoelectricity in 0D, 1D and 2D Zinc Oxide nanostructures. *Ceramics International*, 46(11), 19401–19407. <a href="https://doi.org/10.1016/J.CERAMINT.2020.04.283">https://doi.org/10.1016/J.CERAMINT.2020.04.283</a>
- [27] Li, Z., Yi, X., Yang, J., Bian, L., Yu, Z., & Dong, S. (2022). Designing Artificial Vibration Modes of Piezoelectric Devices Using Programmable, 3D Ordered Structure with Piezoceramic Strain Units. *Advanced Materials*, 34(2). https://doi.org/10.1002/ADMA.202107236
- [28] Lu, L., Ding, W., Liu, J., & Yang, B. (2020). Flexible PVDF based piezoelectric nanogenerators. *Nano Energy*, 78. https://doi.org/10.1016/j.nanoen.2020.105251
- [29] Mahapatra, A., Ajimsha, R. S., Ittoop, M. O., Sharma, A., Karmakar, S., Shaikh, A., Sankar, P. R., & Misra, P. (2023). Flexible Zno:Pvdf Based Free Standing Piezoelectric Nanogenerator for Vibrational Energy Harvesting and Wearable Shoe Insole Pedometer Sensor. SSRN Electronic Journal. https://doi.org/10.2139/SSRN.4358403
- [30] Mahapatra, A., Ajimsha, R. S., & Misra, P. (2022). Oxygen annealing induced enhancement in output characteristics of ZnO based flexible piezoelectric nanogenerators. *Journal of Alloys and Compounds*, 913. https://doi.org/10.1016/J.JALLCOM.2022.165277
- [31] Manjula, Y., Rakesh Kumar, R., Swarup Raju, P. M., Anil Kumar, G., Venkatappa Rao, T., Akshaykranth, A., & Supraja, P. (2020). Piezoelectric flexible nanogenerator based

- on ZnO nanosheet networks for mechanical energy harvesting. *Chemical Physics*, *533*. https://doi.org/10.1016/j.chemphys.2020.110699
- [32] Meng, J., Guo, Z. H., Pan, C., Wang, L., Chang, C., Li, L., Pu, X., & Wang, Z. L. (2021).
  Flexible Textile Direct-Current Generator Based on the Tribovoltaic Effect at Dynamic
  Metal-Semiconducting Polymer Interfaces. ACS Energy Letters, 6(7), 2442–2450.
  <a href="https://doi.org/10.1021/ACSENERGYLETT.1C00288">https://doi.org/10.1021/ACSENERGYLETT.1C00288</a>
- [33] Muhammad, R., Ali, A., Camargo, J., & Castro, M. S. (2020). Temperature Stable Dielectric Properties in BaTiO3–Bi(Mg2/3Nb1/3)O3–NaNbO3 Solid Solution. *ChemistrySelect*, 5(12), 3730–3734. https://doi.org/10.1002/SLCT.202000243
- [34] Nair, K. S., Varghese, H., Chandran, A., Hareesh, U. N. S., Chouprik, A., Spiridonov, M., & Surendran, K. P. (2022). Synthesis of KNN nanoblocks through surfactant-assisted hot injection method and fabrication of flexible piezoelectric nanogenerator based on KNN-PVDF nanocomposite. *Materials Today Communications*, 31, 103291. <a href="https://doi.org/10.1016/J.MTCOMM.2022.103291">https://doi.org/10.1016/J.MTCOMM.2022.103291</a>
- [35] O'Brien, S., Nolan, M. G., Çopuroglu, M., Hamilton, J. A., Povey, I., Pereira, L., Martins, R., Fortunato, E., & Pemble, M. (2010). Zinc oxide thin films: Characterization and potential applications. *Thin Solid Films*, 518(16), 4515–4519. https://doi.org/10.1016/J.TSF.2009.12.020
- [36] Qi, Y., Jafferis, N. T., Lyons, K., Lee, C. M., Ahmad, H., & McAlpine, M. C. (2010). Piezoelectric ribbons printed onto rubber for flexible energy conversion. *Nano Letters*, 10(2), 524–525. https://doi.org/10.1021/NL903377U
- [37] Qian, S., Qin, L., He, J., Niu, X., Qian, J., Mu, J., Geng, W., Hou, X., & Chou, X. (2019a).

  A stretchable piezoelectric elastic composite. *Materials Letters*, 236, 96–100.

  <a href="https://doi.org/10.1016/j.matlet.2018.10.014">https://doi.org/10.1016/j.matlet.2018.10.014</a>

- [38] Qian, S., Qin, L., He, J., Niu, X., Qian, J., Mu, J., Geng, W., Hou, X., & Chou, X. (2019b).

  A stretchable piezoelectric elastic composite. *Materials Letters*, 236, 96–100.

  <a href="https://doi.org/10.1016/J.MATLET.2018.10.014">https://doi.org/10.1016/J.MATLET.2018.10.014</a>
- [39] Shin, D. J., Ji, J. H., Kim, J., Jo, G. H., Jeong, S. J., & Koh, J. H. (2019). Enhanced flexible piezoelectric energy harvesters based on BaZrTiO3–BaCaTiO3 nanoparticles/PVDF composite films with Cu floating electrodes. *Journal of Alloys and Compounds*, 802, 562–572. <a href="https://doi.org/10.1016/j.jallcom.2019.05.363">https://doi.org/10.1016/j.jallcom.2019.05.363</a>
- [40] Shirane, G., Newnham, R., & Pepinsky, R. (1954). Dielectric properties and phase transitions of NaNbO3 and (Na,K)NbO3. *Physical Review*, 96(3), 581–588. https://doi.org/10.1103/PHYSREV.96.581
- [41] Sinha, N., Goel, S., Joseph, A. J., Yadav, H., Batra, K., Gupta, M. K., & Kumar, B. (2018). Y-doped ZnO nanosheets: Gigantic piezoelectric response for an ultra-sensitive flexible piezoelectric nanogenerator. *Ceramics International*, 44(7), 8582–8590. https://doi.org/10.1016/j.ceramint.2018.02.066
- [42] Su, Y., Li, W., Cheng, X., Zhou, Y., Yang, S., Zhang, X., Chen, C., Yang, T., Pan, H., Xie, G., Chen, G., Zhao, X., Xiao, X., Li, B., Tai, H., Jiang, Y., Chen, L. Q., Li, F., & Chen, J. (2022). High-performance piezoelectric composites via β phase programming. *Nature Communications*, *13*(1). https://doi.org/10.1038/S41467-022-32518-3
- [43] Teka, A., Bairagi, S., Shahadat, M., Joshi, M., Ziauddin Ahammad, S., & Wazed Ali, S. (2018). Poly(vinylidene fluoride) (PVDF)/potassium sodium niobate (KNN)–based nanofibrous web: A unique nanogenerator for renewable energy harvesting and investigating the role of KNN nanostructures. *Polymers for Advanced Technologies*, 29(9), 2537–2544. https://doi.org/10.1002/PAT.4365

- [44] Thongsanitgarn, P., Watcharapasorn, A., & Jiansirisomboon, S. (2010). Electrical and mechanical properties of PZT/PVDF 0-3 composites. *Surface Review and Letters*, *17*(1), 1–7. <a href="https://doi.org/10.1142/S0218625X10013540">https://doi.org/10.1142/S0218625X10013540</a>
- [45] Vendrell, X., García, J. E., Bril, X., Ochoa, D. A., Mestres, L., & Dezanneau, G. (2015). Improving the functional properties of (K0.5Na0.5)NbO3 piezoceramics by acceptor doping. *Journal of the European Ceramic Society*, 35(1), 125–130. <a href="https://doi.org/10.1016/j.jeurceramsoc.2014.08.033">https://doi.org/10.1016/j.jeurceramsoc.2014.08.033</a>
- [46] Verma, K., Goel, S., & Sharma, R. (2022). Influence of calcination and sintering temperature on the microstructure, dielectric, ferroelectric and piezoelectric properties of the lead-free KNN ceramics. *Journal of Materials Science: Materials in Electronics*, 33(35), 26067–26085. https://doi.org/10.1007/S10854-022-09295-2
- [47] Verma, K., & Sharma, R. (2022). A flexible piezoelectric generator based on KNN/PVDF composite films: Role of KNN concentration on the piezoelectric performance of generator. *Chinese Journal of Physics*. https://doi.org/10.1016/J.CJPH.2022.12.007
- [48] Vivekananthan, V., Chandrasekhar, A., Alluri, N. R., Purusothaman, Y., Joong Kim, W., Kang, C. N., & Kim, S. J. (2019a). A flexible piezoelectric composite nanogenerator based on doping enhanced lead-free nanoparticles. *Materials Letters*, 249, 73–76. <a href="https://doi.org/10.1016/j.matlet.2019.02.134">https://doi.org/10.1016/j.matlet.2019.02.134</a>
- [49] Vivekananthan, V., Chandrasekhar, A., Alluri, N. R., Purusothaman, Y., Joong Kim, W., Kang, C. N., & Kim, S. J. (2019b). A flexible piezoelectric composite nanogenerator based on doping enhanced lead-free nanoparticles. *Materials Letters*, 249, 73–76. https://doi.org/10.1016/J.MATLET.2019.02.134

- [50] Wang, D., Yuan, G., Hao, G., & Wang, Y. (2018). All-inorganic flexible piezoelectric energy harvester enabled by two-dimensional mica. *Nano Energy*, 43, 351–358. <a href="https://doi.org/10.1016/j.nanoen.2017.11.037">https://doi.org/10.1016/j.nanoen.2017.11.037</a>
- [51] Wang, Z. L., & Song, J. (2006). Piezoelectric nanogenerators based on zinc oxide nanowire arrays. *Science*, *312*(5771), 242–246. https://doi.org/10.1126/SCIENCE.1124005
- [52] Wu, L., Huan, Y., Li, C., Jiang, F., & Wei, T. (2023). Achieving ultrabroad temperature stability range with high dielectric constant and superior energy storage density in KNN–based ceramic capacitors. *Ceramics International*. https://doi.org/10.1016/J.CERAMINT.2023.04.026
- [53] Wu, Y., Abdelwahab, I., Kwon, K. C., Verzhbitskiy, I., Wang, L., Liew, W. H., Yao, K., Eda, G., Loh, K. P., Shen, L., & Quek, S. Y. (2022). Data-driven discovery of high performance layered van der Waals piezoelectric NbOI2. *Nature Communications*, 13(1). https://doi.org/10.1038/S41467-022-29495-Y
- [54] Xu, S., Yeh, Y. W., Poirier, G., McAlpine, M. C., Register, R. A., & Yao, N. (2013a). Flexible piezoelectric PMN-PT nanowire-based nanocomposite and device. *Nano Letters*, *13*(6), 2393–2398. <a href="https://doi.org/10.1021/NL400169T">https://doi.org/10.1021/NL400169T</a>
- [55] Xu, S., Yeh, Y. W., Poirier, G., McAlpine, M. C., Register, R. A., & Yao, N. (2013b). Flexible piezoelectric PMN-PT nanowire-based nanocomposite and device. *Nano Letters*, 13(6), 2393–2398. https://doi.org/10.1021/NL400169T/SUPPL\_FILE/NL400169T\_SI\_001.PDF
- [56] Yadav, H., Sinha, N., Goel, S., & Kumar, B. (2016). Eu-doped ZnO nanoparticles for dielectric, ferroelectric and piezoelectric applications. *Journal of Alloys and Compounds*, 689, 333–341. <a href="https://doi.org/10.1016/j.jallcom.2016.07.329">https://doi.org/10.1016/j.jallcom.2016.07.329</a>

- [57] Yang, W., Zeng, H., Yan, F., Qian, J., Zhu, K., Zhao, K., Li, G., & Zhai, J. (2022).

  Microstructure-driven excellent energy storage NaNbO3-based lead-free ceramics.

  Ceramics International, 48(24), 37476–37482.

  https://doi.org/10.1016/j.ceramint.2022.09.208
- [58] Yaqoob, U., Uddin, A. S. M. I., & Chung, G. S. (2017). A novel tri-layer flexible piezoelectric nanogenerator based on surface- modified graphene and PVDF-BaTiO 3 nanocomposites. *Applied Surface Science*, 405, 420–426. <a href="https://doi.org/10.1016/j.apsusc.2017.01.314">https://doi.org/10.1016/j.apsusc.2017.01.314</a>
- [59] Yue, R., Ramaraj, S. G., Liu, H., Elamaran, D., Elamaran, V., Gupta, V., Arya, S., Verma, S., Satapathi, S., hayawaka, Y., & Liu, X. (2022). A review of flexible lead-free piezoelectric energy harvester. *Journal of Alloys and Compounds*, 918. https://doi.org/10.1016/J.JALLCOM.2022.165653



## 9% Overall Similarity

Top sources found in the following databases:

- 3% Internet database
- Crossref database
- 3% Submitted Works database

- 5% Publications database
- Crossref Posted Content database

#### **TOP SOURCES**

The sources with the highest number of matches within the submission. Overlapping sources will not be displayed.

Komal Verma, Richa Sharma. "A flexible piezoelectric generator based . Crossref	··· 2%
link.springer.com Internet	2%
Brunel University on 2016-05-19 Submitted works	<1%
Qiang Zheng, Bojing Shi, Zhou Li, Zhong Lin Wang. "Recent Progress o	··· <1%
University of Teesside on 2022-05-06 Submitted works	<1%
Abebe Teka, Satyaranjan Bairagi, Md. Shahadat, Mangala Joshi, Sk. Zi	. <1%
Nidhi Sinha, Kriti Batra, Sumit Bhukkal, Ranjan Kumar, Sandeep Kumar,.  Crossref	···· <1%
science.gov Internet	<1%



Higher Education Commission Pakistan on 2021-12-29 Submitted works	<1%
onlinelibrary.wiley.com Internet	<1%
Gurpreet Singh, Moolchand Sharma, Rahul Vaish. "Flexible Ag@LiN	NbO <1%
Rubio-Marcos, F "Effect of ZnO on the structure, microstructure an	nd e <1%
oak.jejunu.ac.kr Internet	<1%
ece.ucf.edu Internet	<1%
Universiti Malaysia Pahang on 2023-01-16 Submitted works	<1%
Coventry University on 2022-04-14 Submitted works	<1%
Sakti Prasanna Muduli, Sushmitha Veeralingam, Sushmee Badhulik Crossref	κα. "I <1%
University of Leeds on 2008-05-21 Submitted works	<1%
eprints.gla.ac.uk Internet	<1%
wikimili.com Internet	<1%





<1%